Unraveling a Nonlinear Coronavirus Model: An Evolutionary Approach to Dynamic Analysis

Muhammad Farhan Tabassum[1,2], Sana Akram[2,3*], Saira Qudus Saggu[4], Ayesha Qudus Saggu[5], Myeda Saeed[5], Saadia Mahmood ul Hassan[1]

[1]*Centre for Skill Development and Leadership, University of Lahore, Lahore, 54000, Pakistan.*
[2]*Department of Mathematics, University of Management and Technology, Lahore, 54000, Pakistan.*
[3]*Department of Mathematics, Lahore Garrison University, Lahore, 54000, Pakistan.*
[4]*MBBS, CHCQM, Riphah International University, Islamabad, Pakistan*
[5]*University Institute of Radiological Sciences and Medical Imaging Technology, Faculty of Allied Sciences, University of Lahore, Lahore, 54000, Pakistan.*
Email: sanaakram@lgu.edu.pk

Abstract:
The COVID-19 epidemic has underlined the vital need of thorough mathematical models to project disease trends and evaluate intervention strategies. Combining vaccination rates (v) and transmission characteristics (\u03b2), this study develops an improved SEIR (Susceptible-Exposed-Infected-Recovered) epidemic model to investigate the spread of COVID-19. By means of stability analysis, we find disease-free and endemic equilibrium points showing that more vaccination coverage significantly reduces the fundamental reproduction number (R_0), hence stabilizing the system. Using the Runge-Kutta method and a novel Evolutionary Padé-Approximation (EPA) approach, which combines Padé rational functions with Differential Evolution optimization to preserve accuracy while following model constraints (positivity, boundedness, and feasibility), numerical solutions are obtained. Even under high transmission conditions ($\beta = 14$), simulations show that improved vaccination speeds the decline of susceptible and infected populations while increasing recoveries, hence lowering R_0 below 1 at 50-100% vaccination rates. Comparative studies of the Runge-Kutta and EPA techniques show notable agreement, hence confirming EPA as a viable substitute for large-scale epidemiological modeling. Our results highlight the vital need of immunization in controlling COVID-19 and provide a computational tool for legislators to strengthen containment initiatives.

Keywords: Optimization; COVID-19 model; Padé approximation; Differential Evolution Algorithm, Reproduction number

1. Introduction

Historically, epidemics and pandemics have devastated people, sometimes causing major historical shifts and the collapse of societies. The ongoing coronavirus pandemic, however, is a dangerous and harmful phenomenon that poses a major threat to mankind [1]. On December 31, 2019, it was first found in Wuhan, Hubei Province, China. The World Health Organization (WHO) designated the disease as a pandemic on March 11, 2020; it was then recognized as the SARS-CoV-2 virus. Scientifically, COVID-19 is a contagious disease that affects humans and produces respiratory sickness. Currently, over 210 countries and territories have recorded cases of coronavirus, which has caused a notable rise in infections [2-3]. Mostly housed by animals, the coronavirus is a zoonotic disease from which humans are

transferred. People with comorbidities including diabetes, heart disease, and asthma—have more susceptibility to serious disease [4].

By April 20, 2020, the World Health Organization reported that COVID-19 had affected almost 2.3 million people, resulting in over 160,000 fatalities connected to the virus [1,2]. Newly reported case rates are rising exponentially and the growth trends fit several mathematical growth functions, including Malthusian and logistic models, which forecast the COVID-19 pandemic scenario [3,5]. Given the seriousness of the situation, notably affected counties and areas have implemented lockdowns, their governments including the WHO urging, pushing, and in some cases ordering people to remain at home to safeguard their citizens. To lower the incidence of fresh cases, experts recommend social separation. Nearly one-third of the world population is now under lockdown. The WHO is promoting awareness and recommending people remain in their own surroundings save for emergencies. At the same time, the WHO is providing relevant information on the pandemic and guidelines for self-protection against the virus [6]. The coronavirus epidemic is beginning to have significant adverse effects on world politics, socio-economics, education, and other important international areas. Every day the medical crisis gets more and more urgent. A mathematical model properly delineating disease transmission is therefore absolutely necessary to help legislators make informed decisions depending on the model's reasonable assumptions. The major damage the epidemic has caused has been linked to a lack of preventive measures and poor decision-making; therefore, we must accept further ignorance on this subject [7-8].

Modeling is the technique of building models that specify buildings and their functional forms. The setup can be changed; usually, in its current state, it is challenging or expensive to change [9]. Epidemiological studies help one to grasp the effects of infectious disease in a population. We do numerical simulations, examine model sensitivity with different parameters, estimate parameters, and assess methods for model building in mathematical modeling. This project intends to track and clarify how diseases spread inside the community. Often called such disease models, infectious diseases are those that spread between people [10–14].

Epidemiology makes great use of mathematical modeling to exactly forecast the effects of an outbreak. Among others, SIS, SIR, and SEIR are the main epidemic models. Often used for several epidemics, the Kermack–McKendrick SIR model is well known [15]. Often, infected people show no visible symptoms, as seen in conditions like chickenpox and tuberculosis; thus, an SEIR model is generally used [16]. The multi-compartment model therefore serves as a vital instrument for forecasting the characteristics of the current, most dangerous sickness.

Coronavirus Disease especially when analytical answers are lacking, epidemiological models are vital for obtaining better developmental insights employing mathematical methodologies grounded on arithmetic and numerical analysis, influence, and derivative mechanisms. Many methods, including traditional analytical and finite difference techniques, do not adequately consider model features such boundedness, positivity, and feasibility. It is absolutely necessary to develop a method that can effectively manage these variables and provide accurate insights into model dynamics.

Reconstituting complicated issues as optimization challenges, several clever meta-heuristics have been created in recent years to address them. [17-18] also shows changes to the differential equations of the proposed metaheuristics; nonetheless, it is not clear how these metaheuristics are used in illness models that are widely dispersed. References [19-23] outline dynamical fractional-order models for epidemic transmission with optimal control. [24-29] also shows recent advances in the pertinent sector. Using evolutionary Padé approximation, Tabassum et al. studied the treatment of the HIV/AIDS epidemic model with vertical transmission [14], thereby extending their work to investigate the basic Nonlinear Coronavirus Model. The results of the present study can be summarized as follows: i) Stability has been calculated and analyzed for equilibrium points, specifically virus equilibrium (VE) and virus-free equilibrium (VFE); ii) The COVID-19 dynamical model has been addressed using a new technique based on Padé Approximation; iii) All required initial conditions, including boundedness, positivity, and feasibility, have been set as constraints; iv) The control equations have been reformulated into a constraint function, and a penalty function method has been used to solve the optimization problem; v) The solution given by this framework is unconditionally convergent to a steady state and satisfies all model requirements.

The nonlinear dynamic Coronavirus model is thoroughly explained in Section 2. Focusing on the Padé technique, differential evolution, penalty function, and the layout of the EPA system for handling the nonlinear epidemiological Coronavirus model, Section 3 The analysis and simulations of the supplied data are the focus of Section 4. The last part covered findings and recommendations for future paths.

2. Dynamical COVID-19 epidemic Model

We want to build a simple yet relevant COVID-19 pandemic model that will produce great analytical outcomes. The disease spreads starting with the introduction of a small group of sick people into a large society. At any time $t \geq 0$, the population (N) is divided into four categories: susceptible (S), exposed and asymptomatic (E), infected (I), and recovered (R). Interaction with an infected person could cause a person vulnerable to infection to get the coronavirus. The infected person might not be able to spread the illness at that time following infection. After a 2-to-14-day period during which the patient is asymptomatic in the incubation stage, he or she can spread disease to a vulnerable person. These people can affect vulnerable people ahead to showing any symptoms, or they may not show symptoms at all. As a result, those without symptoms can spread illness throughout society. Moreover, people are sick yet not contagious throughout the exposure time. Exposed people are not contagious at any one time. Exposed people can spread the disease to the population, though, after a few days. Therefore, for model building we classify the exposed and asymptomatic classes into one compartment. As these people move freely across the population, susceptible could catch illnesses from them [16]. WHO recommendations say that symptomatic infected people will be admitted to hospitals and so will only spread the illness to medical staff members. The exposed and asymptomatic people, however, interact with the broader community and help spread disease.

COVID-19's SEIR model for transmission has four compartments: Susceptible (S), Exposed (E), Infected (I), and Recovered (R). People in an infected group can spread the disease to others. Figure 1 shows the differences in Covid-19 spread among every human community inside the SEIR model. Table 1 defines the variables and parameters of the SEIR model for COVID-19. The temporal change in the numbers of Suspected, Exposed, Infected, and Recovered people within the SEIR mathematical model of Covid-19 transmission can be explained according to the population scheme shown in Figure 1.

Figure 1. Scheme of the Model SEIR transmission for COVID-19

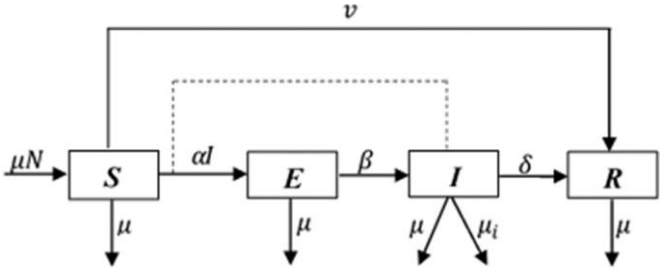

The variables of the model at any time t are defined as:

S(t): Suspected (S) individuals;

E(t): Exposed (E) individuals;

I(t): Infected (I) individuals;

R(t): Recovered (R) individuals.

The model under consideration was purposed by [30] under the form of the following nonlinear system of differential equations:

$$\left.\begin{aligned} \frac{dS}{dt} &= \mu N - (\alpha I + \mu + \nu)S \\ \frac{dE}{dt} &= \alpha IS - (\beta + \mu)E \\ \frac{dI}{dt} &= \beta E - (\mu_i + \delta + \mu)I \\ \frac{dR}{dt} &= \delta I + \nu S - \mu R \end{aligned}\right\} \quad (1)$$

Let $S = \frac{S}{N}, E = \frac{E}{N}, I = \frac{I}{N}, R = \frac{R}{N}$, the above model becomes

$$\left.\begin{aligned} \frac{dS}{dt} &= \mu - (\alpha I + \mu + \nu)S \\ \frac{dE}{dt} &= \alpha IS - (\beta + \mu)E \\ \frac{dI}{dt} &= \beta E - (\mu_i + \delta + \mu)I \\ \frac{dR}{dt} &= \delta I + \nu S - \mu R \end{aligned}\right\} \quad (2)$$

Table 1. Parameter values used in numerical simulations

Parameters	Interpretation	Value [30]
N	Number of human populations	1.5 million
μ	The rate of birth/death population	$\mathbf{6.25 \times 10^{-3}}$
α	Probably of changing from S to E	$\mathbf{0.62 \times 10^{-8}}$
β	Probably of changing from E to I	3,7,14
μ_i	The rate of death population by COVID-19	0.002
δ	Probably of changing from I to R	$\mathbf{6.667 \times 10^{-4}}$
ν	Vaccine of Suspected Population	1, 50, 100%

Based on Eqs. 2, stability analysis is carried out to determine the disease-free equilibrium point and endemic equilibrium point. To determine the two equilibrium points, each equation in above set of equations must be equal to zero or $\frac{dS}{dt} = 0, \frac{dE}{dt} = 0, \frac{dI}{dt} = 0, \frac{dR}{dt} = 0$, we get:

$$\mu - (\alpha I + \mu + \nu)S = 0 \quad (3)$$

$$\alpha IS - (\beta + \mu)E = 0 \quad (4)$$

$$\beta E - (\mu_i + \delta + \mu)I = 0 \quad (5)$$

$$\delta I + \nu S - \mu R = 0 \quad (6)$$

Then, we found the equilibrium point of S, E, I, and R.

Equilibrium points for disease-free are conditions where there is no spread of COVID-19 then, E = I = 0. From Eq. 3 we have $S = \frac{\mu}{(\mu+\nu)}$ and from Eq. 6 we have $R = \frac{\nu}{(\mu+\nu)}$

Then, the Equilibrium points of disease-free for COVID-19 are:

$$K_0 = (S, E, I, R) = \left(\frac{\mu}{(\mu+\nu)}, 0, 0, \frac{\nu}{(\mu+\nu)}\right) \quad (7)$$

The calculated values for *S* and R based on μ = 0.00625 and different values of ν (1%, 50%, and 100%) are as follows:

For ν = 1% then S ≈ 0.9901 and R ≈ 0.0099

For ν = 50% then S ≈ 0.6667 and R ≈ 0.3333

For ν = 100% then S ≈ 0.5 and R ≈ 0.5

Endemic equilibrium points are used to indicate the possibility of disease spread. Because in endemic conditions and disease spread, the population S, E, I, and R ≠ 0. From Eqs. (3) – (6) obtained endemic equilibrium points from COVID-19 are

$$S = \frac{(\mu_i + \delta + \mu)(\beta + \mu)}{\alpha\beta}$$

$$E = \frac{\alpha\beta\mu - (\mu_i + \delta + \mu)(\mu + \nu)}{\alpha\beta}$$

$$I = \frac{\alpha\beta\mu - (\mu_i + \delta + \mu)(\beta + \mu)(\mu + \nu)}{(\mu_i + \delta + \mu)(\beta + \mu)}$$

$$R = \frac{\alpha\beta^2\mu\delta - \beta(\mu_i + \delta + \mu)(\beta + \mu)(\mu + \nu) - \nu\left((\mu_i + \delta + \mu)(\beta + \mu)\right)^2}{\beta\alpha^2(\mu_i + \delta + \mu)(\beta + \mu)}$$

Endemic equilibrium points are

$$K_e = (S^*, E^*, I^*, R^*) = \left(\begin{array}{c} \frac{(\mu_i+\delta+\mu)(\beta+\mu)}{\alpha\beta}, \frac{\alpha\beta\mu-(\mu_i+\delta+\mu)(\mu+\nu)}{\alpha\beta}, \frac{\alpha\beta\mu-(\mu_i+\delta+\mu)(\beta+\mu)(\mu+\nu)}{(\mu_i+\delta+\mu)(\beta+\mu)}, \\ \frac{\alpha\beta^2\mu\delta-\beta(\mu_i+\delta+\mu)(\beta+\mu)(\mu+\nu)-\nu\left((\mu_i+\delta+\mu)(\beta+\mu)\right)^2}{\beta\alpha^2(\mu_i+\delta+\mu)(\beta+\mu)} \end{array}\right) \quad (8)$$

The value of the equilibrium points of the SEIR model is determined by substituting the parametric values from Table 1 and put in Eqs. (3-6) which are equated with zero, then the following system of equation is obtained:

$$548.60625 - (0.0007063\,I(t) + 0.5063)\,S(t) = 0$$

$$(0.0007063\,I(t) + 0.5063)S(t) - 0.07777\,E(t) = 0$$

$$0.0714\,E(t) - 0.006921\,I(t) = 0$$

$$0.006921\,I(t) + 0.5\,S(t) - 0.00625\,R(t) = 0$$

Initial Value of SEIR Model is Suspected individuals are 37500, Exposed individuals are 14000, Infected individuals are 23250 and Recovered individuals are 13250.

The basic reproduction number R_0 is determined using the matrices generation method [9], based on Eqs. (3) – (6). Let $F = \begin{pmatrix} 0 & \alpha S \\ \beta & 0 \end{pmatrix}$ and $V = \begin{pmatrix} (\beta + \mu) & 0 \\ 0 & (\mu_i + \delta + \mu) \end{pmatrix}$ then find V^{-1} and $P = FV^{-1}$

We have $R_0 = \frac{\alpha\beta\mu}{(\mu+\beta)(\mu+\nu)(\mu_i+\delta+\mu)}$ (9)

If $R_0 \leq 1$ then system in Eqs. (3) – (6) of the model is global asymptotic stable otherwise ($R_0 > 1$) is unstable. The basic reproduction number for the endemic case of Covid-19 from Eq. (9) with only 1% vaccination is R_0= 3.2094. This means that, if a person is infected with Covid-19 it will infect 3 other people which shows that the model is unstable. Whereas for other both the cases (50% and 100%) $R_0 < 1$ which means that the model is stable.

Consider a Jacobian matrix

$$J=\begin{bmatrix} -(\alpha I + \mu + \nu) & 0 & \alpha S & 0 \\ \alpha I & -(\beta + \mu) & \alpha S & 0 \\ 0 & \beta & -(\mu_i + \delta + \mu) & 0 \\ \nu & 0 & \delta & -\mu \end{bmatrix} \quad (10)$$

Then find the eigenvalue of the Jacobian matrix in Eq. (9) $\Longrightarrow |\lambda I - J| = 0$.

$$\begin{vmatrix} \lambda + (\alpha I + \mu + \nu) & 0 & -\alpha S & 0 \\ -\alpha I & \lambda + (\beta + \mu) & -\alpha S & 0 \\ 0 & -\beta & \lambda + (\mu_i + \delta + \mu) & 0 \\ -\nu & 0 & -\delta & \lambda + \mu \end{vmatrix} = 0$$

After implication and putting parameter values, the Eigen values that is;

$$\lambda_1 = -0.2166, \lambda_2 = -0.0166, \lambda_3 = -0.0744, \lambda_4 = -7.5395 < 0$$

All the Eigen values are negative which shows that the given system is locally stable.

3. Fundamentals of Padé-approximation and Differential Evolution

3.1. Padé approximation

Through classical theory of continued fractions the idea of a Padé-approximation was introduced at the end of the 19th century. The (N, M) order rational function of Padé approximation is [31]

$$P_{N,M}(t) = \frac{\sum_{i=0}^{N} a_i t^i}{\sum_{j=0}^{M} b_j t^j}$$

The polynomials $\sum_{i=0}^{N} a_i t^i$ and $\sum_{j=0}^{M} b_j t^j$ are known as Padé approximants. By putting $b_0 \neq 0$ normalizing the above expression and attain the following form:

$$P_{N,M}(t) = \frac{\sum_{i=0}^{N} a_i t^i}{1 + \sum_{j=1}^{M} b_j t^j}$$

The above expression contains $(N + M + 1)$ undetermined coefficients, applying the Maclaurin series expansions of $P_{N,M}(t)$ to get the target referred in [31].

3.2. Differential evolution

In 1995 Storn and Price introduced stochastic population-based algorithm named as Differential Evolution (DE) [32], it was simple, robust and reliable to find optimal point. The DE strategy [33] which the most often used is implemented in this paper. The individual set of parameters represented by D dimensional vector. NP represent member in population with vectors $x_i^G, i = 1, 2, \cdots, NP$ and G indicates a generation. During the evolution process the generation remains same. Randomly choose the initial population with uniform distribution. After initialization DE has following three operators:

3.2.1. Initialization

Initial population must be generated for optimization procedure and assigned a randomly chosen value from the boundary constraints:

$$x_{ij}^0 = L_j + rand_j * (U_j - L_j)$$

where $rand_j$ indicates a uniform distribution between $[0, 1]$, L_j is lower and U_j is upper bounds for the j^{th} decision parameter [32].

3.2.2. Mutation

A mutant vector namely v is produced for each target vector x_i^G:

$v_i^{G+1} = x_{r_1}^G + F * \left(x_{r_2}^G - x_{r_3}^G\right), \qquad r_1 \neq r_2 \neq r_3 \neq i$

with randomly chosen indices and $r_1, r_2, r_3 \in \{1, 2, \ldots, NP\}$.

$F \in \mathbb{R}$ which control the amplification of $\left(x_{r_2}^G - x_{r_3}^G\right)$, the value of F must be within the range of $[0, 2]$ [8]. The above indices must be different from each other and also different from the running index i so NP at-leaste four. The new value of this component is generated using if component of a mutation vector exceeds the bounds of search space.

3.2.3. Crossover

To yield the trial vector namely u the following scheme is used, the target vector is mixed with the mutated vector,

$$u_{ij}^{G+1} = \begin{cases} x_{ij}^{G+1}, & \text{rand(j)} \leq CR \quad \text{or} \quad j = \text{randn(i)} \\ v_{ij}^G, & \text{rand(j)} > CR \quad \text{or} \quad j = \text{randn(i)} \end{cases}$$

where $j = 1, 2, \ldots, D$, $\text{rand(j)} \in [0, 1]$ is the j^{th} evaluation of a generator number. Crossover probability constant is $CR \in [0, 1]$. $\text{randn(i)} \in \{1, 2, \ldots, D\}$ is an index which has been randomly chosen, that index confirms that u_i^{G+1} develops at least one element from v_i^{G+1}.

3.2.4. Selection

The selection scheme is as follows:

$$x_i^{G+1} = \begin{cases} u_i^{G+1}, & f\left(u_i^{G+1}\right) < f\left(x_i^G\right) \\ x_i^G, & f\left(u_i^{G+1}\right) \geq f\left(x_i^G\right) \end{cases}$$

If trial vector u_i^{G+1} has a better fitness function value than x_i^G, then u_i^{G+1} is set to x_i^{G+1} . Otherwise, the old value x_i^G is retained due to greedy selection strategy of DE.

3.3. Constraints Handling

To handle constraints the most effective method has been used in the form of penalty function referred in [34]. In penalty function a large positive number depending on degree of violation of constraints is added to the objective function. In the following relation, objective function presented by $\psi(x)$ and the penalty function is presented by $\zeta(x)$ describes penalized function $\varphi(x)$ which was unconstrained defined as follows:

$$\varphi(x) = \begin{cases} \psi(x) + \zeta(x) & \text{if x is infeasible} \\ \psi(x) & \text{ifx is feasible} \end{cases}$$

Here $\zeta(x) \geq 0$ is used for minimization problem and $\zeta(x) \leq 0$ for a maximization problem. There is very rare existence of unconstrained real-world problems generally DE is designed for unconstrained optimization problems. So, this technique converting the constrained optimization problems into unconstrained optimization problems.

3.4 Padé-approximation based Differential Evolution Strategy

The design of the proposed Padé-approximation based Differential Evolution involves the following main steps.

3.4.1. Padé approximation based residual function

Suppose that $S(t), I(t), C(t)$ and $A(t)$ are approximated by Padé rational functions as

$$S(t) \approx \frac{\sum_{i=0}^{N} a_i t^i}{1+\sum_{j=1}^{M} b_j t^j}, \qquad I(t) \approx \frac{\sum_{i=0}^{N} c_i t^i}{1+\sum_{j=1}^{M} d_j t^j}, \qquad C(t) \approx \frac{\sum_{i=0}^{N} e_i t^i}{1+\sum_{j=1}^{M} f_j t^j} \qquad A(t) \approx \frac{\sum_{i=0}^{N} g_i t^i}{1+\sum_{j=1}^{M} h_j t^j},$$

Imposing initial conditions

$S(t_0) = S_0, I(t_0) = I_0, C(t_0) = C_0, \text{ and } A(t_0) = A_0$

we obtain

$a_0 = S_0, c_0 = I_0, e_0 = C_0, g_0 = A_0$

(11)

The discrete time steps are $t_q = t_0 + qh;\ q = 0, 1, 2, 3, \ldots, q_{max}$, and the above system of equations (3) reduces as:

$$\left.\begin{aligned} \varepsilon_1(t_q) &= 0 \\ \varepsilon_2(t_q) &= 0 \\ \varepsilon_3(t_q) &= 0 \\ \varepsilon_4(t_q) &= 0 \end{aligned}\right\}$$

(12)

Here ε_1, ε_2, ε_3 and ε_4 are the residuals defined by

$$\varepsilon_1(t_q) = \left(1 + \sum_{j=1}^{M} b_j t_q^j\right)\left(\sum_{i=0}^{N} i a_i t_q^{i-1}\right) - \left(\sum_{i=0}^{N} a_i t_q^i\right)\left(\sum_{j=1}^{M} j b_j t_q^{j-1}\right) - X_1(t_q)\left(1 + \sum_{j=1}^{M} b_j t_q^j\right)^2 \quad (13)$$

$$\varepsilon_2(t_q) = \left(1 + \sum_{j=1}^{M} d_j t_q^j\right)\left(\sum_{i=0}^{N} i c_i t_q^{i-1}\right) - \left(\sum_{i=0}^{N} c_i t_q^i\right)\left(\sum_{j=1}^{M} j d_j t_q^{j-1}\right) - X_2(t_q)\left(1 + \sum_{j=1}^{M} d_j t_q^j\right)^2 \quad (14)$$

$$\varepsilon_3(t_q) = \left(1 + \sum_{j=1}^{M} f_j t_q^j\right)\left(\sum_{i=0}^{N} i e_i t_q^{i-1}\right) - \left(\sum_{i=0}^{N} e_i t_q^i\right)\left(\sum_{j=1}^{M} j f_j t_q^{j-1}\right) - X_3(t_q)\left(1 + \sum_{j=1}^{M} f_j t_q^j\right)^2 \quad (15)$$

$$\varepsilon_4(t_q) = \left(1 + \sum_{j=1}^{M} h_j t_q^j\right)\left(\sum_{i=0}^{N} i g_i t_q^{i-1}\right) - \left(\sum_{i=0}^{N} g_i t_q^i\right)\left(\sum_{j=1}^{M} j h_j t_q^{j-1}\right) - X_4(t_q)\left(1 + \sum_{j=1}^{M} h_j t_q^j\right)^2 \quad (16)$$

By solving system (12) having $4q_{max}$ nonlinear simultaneous equations the problem reduces to finding 4(M + N) coefficients of Padé approximants.

3.4.2. Objective Function

Suppose that

$$x = \begin{pmatrix} a_1, a_2, \cdots, a_M, b_1, b_2, \cdots, b_N, c_1, c_2, \cdots, c_M, d_1, d_2, \cdots, d_N, \\ e_1, e_2, \cdots, e_M, f_1, f_2, \cdots, f_N, g_1, g_2, \cdots, g_M, h_1, h_2, \cdots, h_N, \end{pmatrix}^t \in \mathbb{R}^{4(M+N)},$$

by converting the system into minimization problem as:

$$\text{Minimize } \phi(x) = \frac{1}{4}\sum_{z=1}^{4}\sum_{q=0}^{q_{max}}\left[\varepsilon_z(t_q)\right]^2 \quad (17)$$

3.4.3. Problem Constraints

The equality constraints of the model are considered as:

$$h_1(t) = S(t) - S_0 = 0 \quad (18)$$

$$h_2(t) = I(t) - I_0 = 0 \quad (19)$$

$$h_3(t) = C(t) - C_0 = 0 \quad (20)$$

$$h_4(t) = A(t) - A_0 = 0 \quad (21)$$

The inequality constraints (22) to (25) are related to positivity

$$g_{1q} = \frac{\sum_{i=0}^{N} a_i t_q^i}{1+\sum_{j=1}^{M} b_j t_q^j}, \quad (22)$$

$$g_{2q} = \frac{\sum_{i=0}^{N} c_i t_q^i}{1+\sum_{j=1}^{M} d_j t_q^j}, \quad (23)$$

$$g_{3q} = \frac{\sum_{i=0}^{N} e_i t_q^i}{1+\sum_{j=1}^{M} f_j t_q^j}, \quad (24)$$

$$g_{4q} = \frac{\sum_{i=0}^{N} g_i t_q^i}{1+\sum_{j=1}^{M} h_j t_q^j}, \quad (25)$$

whereas (26) incorporates the bounded-ness of the numerical solution.

$$g_{1q} + g_{2q} + g_{3q} + g_{4q} \leq \Lambda/\mu \quad (26)$$

3.4.4. Penalty Function

By using the following penalty function methodology unconstrained optimization model is obtained:

$$\zeta(x) = \sum_{q=1}^{q_{max}} P_q \times \max\left\{0, (h_1)^2, (h_2)^2, (h_3)^2, (h_4)^2, -g_{1q}, -g_{2q}, -g_{3q}, -g_{4q}, \sum_{s=1}^{4} g_{sq} - \Lambda/\mu\right\}$$

Here scalar Pq is a large positive real number of q^{th} discrete time step acting as a penalty factor then the unconstrained objective function is

$$\text{Minimize } \varpi(x) = \phi(x) + \zeta(x) \quad (27)$$

3.4.5. Optimization Process with Differential Evolution

The following steps are involved to optimize objective function (27) through EPA scheme as:

Step 1. Generate population randomly, population of K solutions $x_j \in \mathbb{R}^{4(M+N)}; 1 \leq j \leq K$.

Step 2. Evaluate the value $\varpi_j = \varpi(x_j)$ of each solution. Collect the best solution with the minimum value of objective function. Initially set T = 0.

Step 3. Set T = T + 1.

Step 4. Choose three distinct solutions x_A, x_B and x_C from the population excluding x_j for each of $j = 1, 2, 3, \ldots, K$, Set y = x_j.

Step 5. For each of the dimensions $i = 1, 2, 3, \ldots, 4(M + N)$, alter the i^{th} coordinate according to

$$y_i = \begin{cases} x_{Ai} + F \times (x_{Bi} - x_{Ci}) & \text{if rand} < CR \\ x_{ji} & \text{otherwise} \end{cases}$$

Step 6. If $\varpi(y) < \varpi_j$ then $x_j \leftarrow y$, otherwise discard y.
Step 7. Best solution must be update.
Step 8. If T > number of iterations, then terminate, by maintaining the best solution, otherwise repeat all the process from step 3.

4. Numerical Results

Set parameters of DE algorithm for numerical illustrations: $N = 50;\ F = 0.55; CR = 0.91$ and maximum iterations $= 2000$. The approximation order for Padé is set to $(N, M) = (2, 2)$. The q_{max} parameter is set to 2000. The penalty factor for all q is set to $L_q = 10^{10}$. The optimized COVID-19 model parameters are given in Table 1. In all simulations 100 independent runs have been taken and chosen the best one, Intel Core i7 with 8GB RAM computer was used for experimentation with Microsoft windows 11. The source code was executed by using MATLAB (R2023b). The mathematical analysis of the non-linear epidemic COVID-19 model was provided. To notice the sound effects of the EPA algorithm on susceptible, infected and recovered population having the property of uniqueness and positivity.

Table 2. The values of equilibrium point, eigen value and R_0

Simulation	β	v	λ_1	λ_2	λ_3	λ_4	S*	E*	I*	R*	R_0
1	3	1%	-0.217	-0.017	-0.074	-7.54	0.99	0.0253	0.03964	0.01	3.2
2	3	50%	-0.201	-0.016	-0.072	-7.522	0.667	0.03329	0.01659	0.333	0.7
3	3	100%	-0.19	-0.015	-0.07	-7.504	0.5	0.03347	0.02327	0.5	0.7
4	7	1%	-0.217	-0.017	-0.074	-7.54	0.99	0.01737	0.02404	0.01	4.3
5	7	50%	-0.204	-0.016	-0.073	-7.521	0.667	0.02871	0.01229	0.333	0.7
6	7	100%	-0.191	-0.016	-0.071	-7.505	0.5	0.02789	0.03363	0.5	0.5
7	14	1%	-0.217	-0.017	-0.074	-7.54	0.99	0.03048	0.03738	0.01	5.1
8	14	50%	-0.2	-0.016	-0.073	-7.521	0.667	0.03805	0.01354	0.333	0.5
9	14	100%	-0.189	-0.015	-0.07	-7.505	0.5	0.03269	0.01013	0.5	0.4

Table 2 presents the results of nine simulations across different transmission rates (β) and vaccination coverage levels (v). Each simulation enumerates eigenvalues (λ_1 to λ_4), equilibrium values for susceptible (S*), exposed (E*), infected (I*), and recovered (R*) people, in addition to the fundamental reproduction number (R_0). All eigenvalues in the simulations are negative, signifying that the system attains a stable equilibrium in each instance.

Analysis of the results indicates that a low vaccination rate (1%) coupled with reduced transmission rates (β = 3) yields a notably high R_0 value of 3.21, implying that the infection remains prevalent among the population. With vaccination rates reaching 50% and 100%, R_0 decreases to 0.72 and 0.65, respectively, signifying that the disease will progressively extinguish. A same pattern is noted for β = 7. with 1% vaccination, R_0 is 4.25, indicating a significant possibility for ongoing transmission; however, with 50% and 100% vaccination, R_0 decreases to 0.65 and 0.5 respectively, effectively managing the outbreak. At the maximum transmission rate (β = 14), R_0 reaches its peak at 5.1 with merely 1% vaccination, indicating a substantial pandemic potential. Increasing vaccine coverage to 50% and 100% dramatically reduces R_0 to 0.45 and 0.4, respectively, indicating effective epidemic control.

In all scenarios, increased vaccination coverage consistently results in reduced R_0 values, irrespective of the transmission rate. Complete vaccination (100%) decreases R_0 well below 1, even in the presence of a high transmission rate, underscoring the vital role of vaccination in epidemic management. Furthermore, the equilibrium values indicate that increased vaccination correlates with a reduction in the proportion of susceptible persons (S*) and an augmentation in the proportion of recovered individuals (R*), hence affirming the efficacy of vaccination programs. The data unequivocally demonstrate that vaccination is an effective instrument for managing infectious illnesses, especially in contexts of elevated transmission rates.

Figure 2. Variation in the number of populations Exposed (E) for different values of β, solid line is for Runge Kutta method and dotted line is for EPA

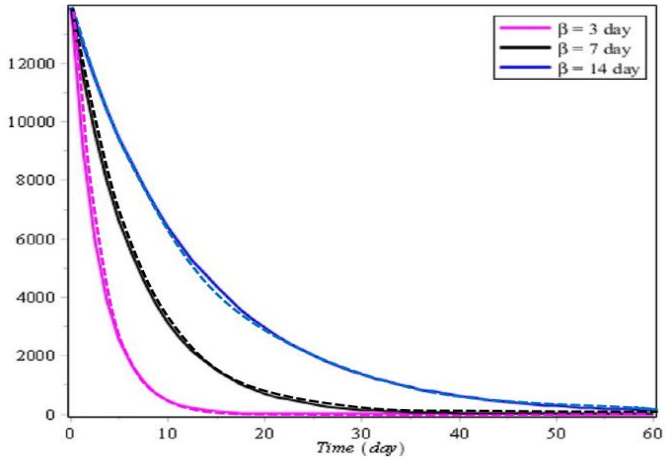

The figure 2 illustrates the temporal variation in the count of exposed individuals (E) for distinct values of β (3, 7, and 14 days). The x-axis denotes time in days, whilst the y-axis indicates the quantity of exposed persons. For each β value, three curves are depicted, with the solid line denoting the Runge-Kutta approach and the dotted line indicating the EPA method. It is noted that with a smaller β (β = 3 days), the quantity of exposed persons diminishes swiftly, approaching zero in approximately 15 days. For β = 7 days, the fall is more gradual than for β = 3 days, and for β = 14 days, the reduction is even less pronounced, with a considerable percentage of exposed individuals remaining after 40–50 days. This signifies that a diminished β facilitates a more rapid decline in the exposed population, whilst an augmented β yields a more gradual reduction. Furthermore, a comparison of the findings from the Runge-Kutta and EPA approaches reveals that the solid and dotted lines closely align across all β values. This indicates that both procedures yield nearly comparable outcomes, with the EPA method offering a dependable approximation of the more accurate Runge-Kutta solution.

Figure 3. Variation in the number of populations Infected (I) for different values of β, solid line is for Runge Kutta method and dotted line is for EPA

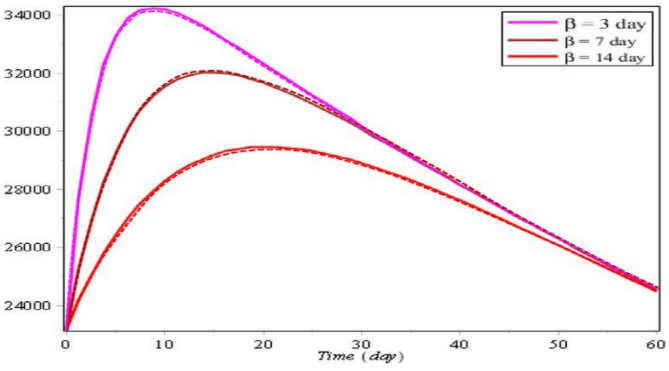

Figure 3 illustrates the fluctuation in the number of infected individuals (I) over time for various values of β (3, 7, and 14 days). The x-axis denotes time in days, whilst the y-axis indicates the quantity of infected persons. For each β value, two curves are depicted: the solid line signifies the Runge-Kutta approach, while the dotted line denotes the EPA method. It is noted that for all β values, the count of infected persons initially rises, attaining a zenith before progressively diminishing. When β is 3 days, the infected population escalates rapidly, attaining a higher apex approximately on day 10. For β = 7 days, the peak is diminished and occurs later, whilst for β = 14 days, the peak is further reduced and transpires after an extended duration. A smaller β results in a more rapid and extensive epidemic, whereas a bigger β yields a slower transmission with a reduced peak of infected persons. The results of the Runge-Kutta and EPA approaches exhibit a tight proximity, with the solid and dotted lines for each β value nearly overlapping. This indicates that both methods yield comparable results, with the EPA method functioning as a dependable approximation of the more precise Runge-Kutta solution.

Figure 4. Variation in the number of populations Suspected (S) for different values of ν, solid line is for Runge Kutta method and dotted line is for EPA

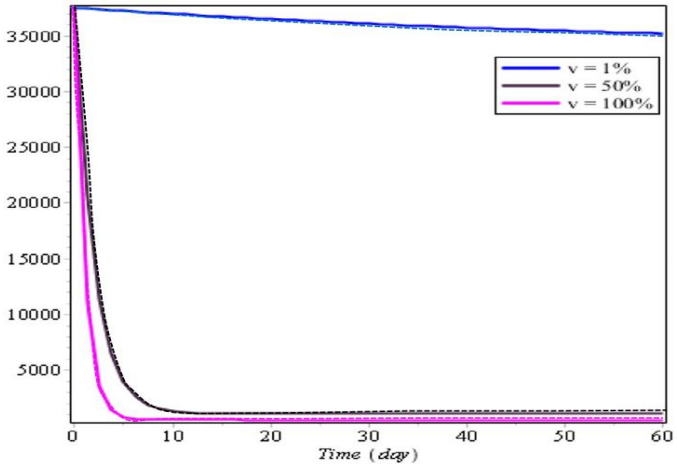

Figure 4 illustrates the fluctuation in the quantity of suspicious persons (S) over time for various values of ν (1%, 50%, and 100%). The x-axis denotes time in days, whilst the y-axis indicates the quantity of suspected individuals. Each ν value is represented by two curves: a solid line for the Runge-Kutta method and a dashed line for the EPA method. When ν is 100%, the number of suspected persons diminishes fast, becoming zero within around 10 days. At ν = 50%, the decline is more gradual than at 100%, yet remains swift, with the presumed population experiencing a substantial reduction within the initial 15 days. Nevertheless, when ν is merely 1%, the reduction is significantly more gradual, and a substantial percentage of suspected persons persist even after 60 days. A larger ν value correlates with a more rapid removal or transformation of the suspicious population, whereas a lower ν yields a longer reduction. The comparison of results from the Runge-Kutta and EPA approaches reveals that the solid and dotted lines are remarkably close for all ν values, signifying that both methods provide highly analogous outcomes. Consequently, the EPA technique offers a dependable estimation of the more precise Runge-Kutta method.

Figure 5. Variation in the number of populations Recovered (R) for different values of ν, solid line is for Runge Kutta method and dotted line is for EPA

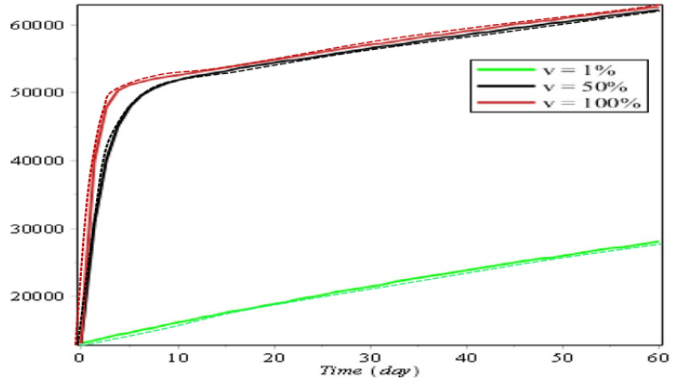

The figure shows how the number of recovered people changes over 60 days for three different recovery rates (ν = 1%, 50%, and 100%). The solid lines represent the Runge-Kutta method, a precise numerical technique, while the dotted lines show results from the EPA method, which may use simpler approximations. When ν is higher (100%), the recovery count rises quickly, reaching the highest number of recovered individuals. In contrast, a lower ν (1%) leads to a much slower and smaller increase in recoveries. The Runge-Kutta method produces smooth, continuous curves, indicating accurate calculations. On the other hand, the EPA method's dotted lines are slightly less smooth, suggesting minor differences due to approximation. Overall, both methods agree on the general trend higher ν means faster and more recoveries but the Runge-Kutta method is more precise. The EPA method, while potentially less accurate, might be simpler and faster for certain applications. The choice between them depends on whether precision or computational efficiency is more important.

5. Conclusion

This research examined COVID-19 transmission with a modified SEIR model that integrates vaccination rates and transmission factors. Our findings indicate that elevated vaccination coverage (50-100%) successfully mitigates outbreaks by decreasing the reproduction number below 1, whereas little vaccination (1%) results in unchecked transmission. The analysis indicated that accelerated disease transmission results in swifter outbreaks and more rapid reductions in cases. We corroborated our methodology by juxtaposing the exact Runge-Kutta method with our efficient EPA algorithm, demonstrating that both yield dependable outcomes. The study has significant limitations: it assumes homogenous population mixing, fails to consider age-related susceptibility variations, and excludes factors such as decreasing immunity and emerging mutations. These simplifications may influence practical applicability. We propose that future study expand the model to incorporate age-stratified populations, regional transmission dynamics, and temporally variable parameters for immunity duration. The integration of real-time data assimilation and machine learning methodologies may improve forecast precision. Furthermore, examining socioeconomic determinants affecting vaccine adoption and the effects of non-pharmaceutical treatments might yield more thorough policy insights. This study lays the groundwork for advanced epidemiological modeling that can enhance public health strategies during present and future pandemics.

References

[1]K Worldometer. (n.d.). Coronavirus update. Retrieved April 26, 2025, from https://www.worldometers.info/coronavirus/

[2] World Health Organization. (n.d.). Coronavirus disease (COVID-19) pandemic. Retrieved April 26, 2025, from https://www.who.int/emergencies/diseases/novel-coronavirus-2019

[3] Kamrujjaman, M., Mahmud, M. S., & Islam, M. S. (2020). Coronavirus outbreak and the mathematical growth map of COVID-19. Annual Research & Review in Biology, 35(1), 72–78. https://doi.org/10.9734/arrb/2020/v35i130182

[4] Ahmad, T., Khan, M., Khan, F. M., & Hui, J. (2020). COVID-19: Zoonotic aspects. Travel Medicine and Infectious Disease, 36, 101632. https://doi.org/10.1016/j.tmaid.2020.101632

[5] Volpert, V., Banerjee, M., & Petrovskii, S. (2020). On a quarantine model of coronavirus infection and data analysis. Mathematical Modelling of Natural Phenomena, 15, 24. https://doi.org/10.1051/mmnp/2020011

[6] Vialatte, N., Lemoine, V., Cledat, R., et al. (2014). Mathematical modeling of human behaviors during catastrophic events. In Proceedings of the 4th International Conference on Complex Systems and Applications (ICCSA2014) (pp. 67–74). Le Havre, France.

[7] Ivorra, B., & Ramos, A. M. (2020). Application of the BE-CODIS mathematical model to forecast the international spread of the 2019–20 Wuhan coronavirus outbreak. https://doi.org/10.13140/RG.2.2.31460.94081

[8] Mahmud, M. S., Kamrujjaman, M., Adan, M. M. I. Y., Hossain, M. A., Rahman, M. M., Islam, M. S., et al. (2022). Vaccine efficacy and SARS-CoV-2 control in California and U.S. during the session 2020–2026: A modeling study. Infectious Disease Modelling, 7(1), 62–81. https://doi.org/10.1016/j.idm.2021.11.002

[9] Guyton, A. C., & Hall, J. E. (1991). Textbook of medical physiology (8th ed.). Philadelphia: W. B. Saunders.

[10] Tabassum, M. F., Farman, M., Akgül, A., & Akram, S. (2022). Mathematical treatment of nonlinear pine wilt disease model: An evolutionary approach. Punjab University Journal of Mathematics, 54(9), 607–620.

[11] Tabassum, M. F., Akgül, A., Akram, S., Farman, M., Karim, R., & Mahmood ul Hassan, S. (2022). Treatment of dynamical nonlinear measles model: An evolutionary approach. International Journal of Nonlinear Analysis and Applications, 13(1), 1629–1638. https://doi.org/10.22075/ijnaa.2020.20450.2156

[12] Farman, M., Tabassum, M. F., Naik, P. A., & Akram, S. (2020). Numerical treatment of a nonlinear dynamical hepatitis-B model: An evolutionary approach. European Physical Journal Plus, 135(12), 941. https://doi.org/10.1140/epjp/s13360-020-00902-x

[13] Tabassum, M. F., Saeed, M., Chaudhry, N. A., & Akram, S. (2020). Treatment of non-linear epidemiological smoking model using evolutionary Padé-approximation. Proceedings of the Pakistan Academy of Sciences, 57(2), 11–19.

[14] Tabassum, M. F., Saeed, M., Akgül, A., Farman, M., & Chaudhry, N. A. (2020). Treatment of HIV/AIDS epidemic model with vertical transmission by using evolutionary Padé-approximation. Chaos, Solitons & Fractals, 134, 109686. https://doi.org/10.1016/j.chaos.2020.109686

[15] Kermack, W. O., & McKendrick, A. G. (1927). A contribution to the mathematical theory of epidemics. Proceedings of the Royal Society A, 115(772), 700–721. https://doi.org/10.1098/rspa.1927.0118

[16] Castillo-Chavez, C., & Feng, Z. (1996). Mathematical models for the disease dynamics of tuberculosis. In Advances in Mathematical Population Dynamics: Molecules, Cells and Man (pp. 1–28).
[17] Ara, A., et al. (2018). Wavelets optimization method for evaluation of fractional partial differential equations: An application to financial modelling. Advances in Difference Equations, 2018(1), 8. https://doi.org/10.1186/s13662-017-1461-2
[18] Panagant, N., & Bureerat, S. (2014). Solving partial differential equations using a new differential evolution algorithm. Mathematical Problems in Engineering, 2014, 747490. https://doi.org/10.1155/2014/747490
[19] Naik, P. A., Zu, J., & Owolabi, K. M. (2020). Global dynamics of a fractional order model for the transmission of HIV epidemic with optimal control. Chaos, Solitons & Fractals, 138, 109826. https://doi.org/10.1016/j.chaos.2020.109826
[20] Qureshi, S., & Atangana, A. (2019). Mathematical analysis of dengue fever outbreak by novel fractional operators with field data. Physica A: Statistical Mechanics and its Applications, 526, 121127. https://doi.org/10.1016/j.physa.2019.121127
[21] Naik, P. A., et al. (2020). Chaotic dynamics of a fractional order HIV-1 model involving AIDS-related cancer cells. Chaos, Solitons & Fractals, 140, 110272. https://doi.org/10.1016/j.chaos.2020.110272
[22] Noeiaghdam, S., & Araghi, M. A. F. (2020). A novel approach to find optimal parameter in the homotopy-regularization method for solving integral equations. Applied Mathematics, 14(1), 99–107.
[23] Noeiaghdam, S., Araghi, M. A. F., & Abbasbandy, S. (2020). Valid implementation of Sinc-collocation method to solve the fuzzy Fredholm integral equation. Journal of Computational and Applied Mathematics, 370, 112632. https://doi.org/10.1016/j.cam.2019.112632
[24] Araghi, M. A. F., & Noeiaghdam, S. (2017). Fibonacci-regularization method for solving Cauchy integral equations of the first kind. Ain Shams Engineering Journal, 8(3), 363–369. https://doi.org/10.1016/j.asej.2015.10.011
[25] Qureshi, S., & Atangana, A. (2020). Fractal-fractional differentiation for the modeling and mathematical analysis of nonlinear diarrhea transmission dynamics under the use of real data. Chaos, Solitons & Fractals, 136, 109812. https://doi.org/10.1016/j.chaos.2020.109812
[26] Qureshi, S. (2020). Periodic dynamics of rubella epidemic under standard and fractional Caputo operator with real data from Pakistan. Mathematics and Computers in Simulation, 178, 151–165. https://doi.org/10.1016/j.matcom.2020.06.001
[27] Mansal, F., & Sene, N. (2020). Analysis of fractional fishery model with reserve area in the context of time-fractional order derivative. Chaos, Solitons & Fractals, 140, 110200. https://doi.org/10.1016/j.chaos.2020.110200
[28] Sene, N. (2020). Stability analysis of the fractional differential equations with the Caputo-Fabrizio fractional derivative. Journal of Fractional Calculus and Applications, 11(2), 160–172.
[29] Sene, N. (2020). Fractional diffusion equation with new fractional operator. Alexandria Engineering Journal, 59(4), 2907–2914. https://doi.org/10.1016/j.aej.2020.04.021
[30] Annas, S., Pratama, M. I., Rifandi, M., Sanusi, W., & Side, S. (2020). Stability analysis and numerical simulation of SEIR model for pandemic COVID-19 spread in Indonesia. Chaos, Solitons & Fractals, 139, 110072. https://doi.org/10.1016/j.chaos.2020.110072
[31] Vajta, M. (2000). Some remarks on Padé-approximations. In Proceedings of the 3rd TEMPUS-INTCOM Symposium.
[32] Price, K., Storn, R. M., & Lampinen, J. A. (2006). Differential evolution: A practical approach to global optimization. Springer Science & Business Media. https://doi.org/10.1007/3-540-31306-0
[33] Brest, J., Greiner, S., Boskovic, B., Mernik, M., & Zumer, V. (2006). Self-adapting control parameters in differential evolution: A comparative study on numerical benchmark problems. IEEE Transactions on Evolutionary Computation, 10(6), 646–657. https://doi.org/10.1109/TEVC.2006.872133
[34] Coello Coello, C. A., & Montes, E. M. (2002). Constraint-handling in genetic algorithms through the use of dominance-based tournament selection. Advanced Engineering Informatics, 16(3), 193–203. https://doi.org/10.1016/S1474-0346(02)00011-3